Morphological Analysis of Highly Filled Propylene/Ethylene Copolymers

L. L. Ionescu-Vasii,[1] Paula M. Wood-Adams,[1]* Eric Duchesne,[2] Gilles L'Espérance,[2] Teresa Karjala,[3] Patricia Ansems[3]

[1]*Department of Mechanical and Industrial Engineering, Concordia University, Montréal, Canada*
[2]*Centre for Characterization and Microscopy of Materials, École Polytechnique de Montréal, Montréal, Canada*
[3]*Performance Plastics & Chemicals, Dow Chemical Company, Freeport, Texas*

Received 19 June 2006; accepted 2 November 2006
DOI 10.1002/app.26448
Published online 11 June 2007 in Wiley InterScience (www.interscience.wiley.com).

ABSTRACT: A series of particulate composites based on a new family of propylene/ethylene (P/E) copolymers produced by Dow Chemical Co. were studied with microscopy and differential scanning calorimetry (DSC). To understand the good processability exhibited by the composites, we studied the composite microstructure and the bulk rheological properties. Here we report the results of a study of the microstructure and thermal behavior. Electron micrographs of the composites showed a uniform dispersion of the particles in the copolymer matrices at all experimental concentrations with very little particle agglomeration. The images suggested low adhesion between the matrices and the particles. The copolymers were semicrystalline, and their morphologies changed with the ethylene content. An increase in the ethylene content led to a decrease in the crystallinity and changes in the shape and size of the crystallites. Tapping-mode atomic force microcopy images of a 9 wt % ethylene copolymer contained spherulites, lamellae, and a crosshatched structure characteristic of α-isotactic polypropylene. The crosshatched structure was not present at higher ethylene contents. A DSC study of the pure copolymers and their composites revealed that only very small modifications to the thermal behavior of the P/E copolymers were induced by calcium carbonate particles. J Appl Polym Sci 105: 3757–3772, 2007

Key words: atomic force microscopy (AFM); composites; crystal structures; differential scanning calorimetry; electron microscopy

INTRODUCTION

Discoveries in the area of polymer synthesis[1–7] have resulted in the possibility of designing and synthesizing a wide variety of polymers with unusual properties. Recently, Dow Chemical Co. developed a new technology that allows the copolymerization of propylene with various α-olefin comonomers over a broad range of compositions in an isotactic fashion and with a high molecular weight. New propylene/ethylene (P/E) copolymers produced with this technology have ethylene contents ranging from 0 to 19 wt % and exhibit a unique molecular structure and as a result excellent physical and mechanical properties.[8] These new P/E copolymers have polydispersity indices between 2 and 3.2 and broad crystallinity distributions and allow high filler loadings (>80 wt %) while maintaining good processability.

Correspondence to: P. M. Wood-Adams (woodadam@alcor.concordia.ca).
**Present address:* Department of Mechanical and Industrial Engineering, Concordia University, 1455 de Maisonneuve Blvd. West, EV004. 251, Montréal, Québec, H3G 1M8, Canada.

Journal of Applied Polymer Science, Vol. 105, 3757–3772 (2007)

These copolymers have previously been classified according to their mechanical properties.[8] As the ethylene content increases, their behavior changes from that of a typical thermoplastic to plastomeric, elastoplastomeric, and finally elastomeric behavior. These changes in the mechanical properties result from the morphology changing because of the presence of the ethylene units, which disrupt the crystal formation. The materials studied here belong to the elastoplastomer and elastomer categories.

Minerals such as calcium carbonate ($CaCO_3$) are often incorporated as particulate fillers into polymers to both modify the solid-state properties and to reduce the cost. The end properties of such composites are usually intermediate between the two components and depend on the filler content, its size and shape, its dispersion, and the interface between the inorganic filler and the polymer matrix. The maximum end filler content is often determined more by the processing considerations than the use properties. Usually, the filled polymer melts have very high viscosities and as a result poor processability. Therefore, from an industrial point of view, the high loading capacity of a polymer matrix has an important impact on both the economics and end-use properties of its composites based on the polymer.

Our activity focuses on the study of the new P/E copolymers and their composites with treated $CaCO_3$. Our goal is to develop a fundamental understanding of the microstructure and properties of these filled copolymers to find the optimal processing conditions for the composites and to provide information for the design of new polymer matrices with a similar or even better capacity for incorporating particles. This can be possible only if we correlate the information about the polymer molecular structure, the particle surface treatment, the composite microstructure, and the bulk properties.

We report here the results of our study by different microscopy techniques of the microstructure of 12 composites based on the new P/E copolymers filled with treated $CaCO_3$. A differential scanning calorimetry (DSC) study was also performed to provide additional information. The objectives of this study were to obtain information about the following:

1. The shape and size of the $CaCO_3$ particles and their dispersion in the polymer matrices.
2. The morphology of the polymer matrices.
3. The impact of $CaCO_3$ particles on the morphology of the polymer matrices.
4. The contact between the $CaCO_3$ particles and the polymer matrices.

EXPERIMENTAL

Materials

Three isotactic P/E copolymers with different ethylene contents (9, 12, and 15 wt %; Table I) and 12 composites of these copolymers (20, 40, 60, and 80 wt % $CaCO_3$) were studied. Here we have named the polymers P/E-x, where x refers to the ethylene content (wt %). The $CaCO_3$, Film Link 400, used in the preparation of the composites was supplied by Imerys. The particle specific surface area was between 4 and 5 m^2/g. The particles were coated with stearate (one stearate molecule per 25 $Å^2$) via a heated air-swept process. The surface coating on the $CaCO_3$ was slightly less than a monolayer.

TABLE I
Characteristics of the Three P/E Copolymers

Ethylene (wt %)	M_w (g/mol)[a]	M_w/M_n[b]	Density (g/cm^3)[c]
9	143,800	3.17	0.8765
12	141,500	2.85	0.8671
15	133,000	2.79	0.8597

[a] Weight-average molecular weight.
[b] Weight-average molecular weight/number-average molecular weight.
[c] Measured according to ASTM D 792.

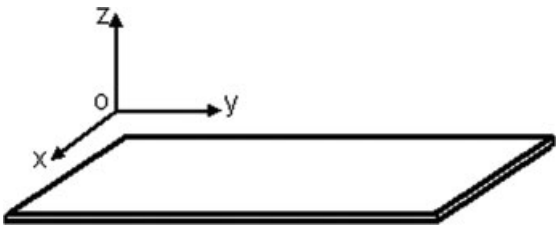

Figure 1 Schematic representation of a composite sheet used for the preparation of samples investigated by microscopy.

Composite preparation

The polymer and the filler ($CaCO_3$ particles treated with stearic acid) were dry-blended in the desired ratio so that the mixture filled 58.5% (181.5 cc) of the mixer bowl (Rheomix 3000, Haake). The dry-blended components were added to the preheated Haake bowl (190°C) with rotors at 30 rpm through a funnel that allowed the material to be added all at once, rammed into the bowl, and sealed. The components were allowed to melt and mix for 15–20 min while the torque and melt temperature were graphically observed. Mixing was assumed to be complete when the torque signal was constant. The rotors were then stopped, and the blended mass was removed, pressed into a patty with a manually operated hydraulic compression press, and then cooled. The sample was then cut into smaller pieces for storage and later compression-molded at 204°C into $15 \times 23 \times 0.13$ cm^3 sheets. Figure 1 shows the schematic representation of a composite sheet used for the preparation of samples analyzed by microscopic techniques.

Analysis techniques and sample preparation

Several microscopic and sample preparation techniques were used to characterize the microstructure of the composites.

Scanning electron microscopy (SEM)

The SEM experiments were carried out with a JEOL JSM 840 scanning electron microscope (Tokyo, Japan) operated at acceleration voltages of 5, 12, and 15 kV. Images of the $CaCO_3$ powder and cross sections of the polymer composite sheets were recorded by this method. $CaCO_3$ was fixed on a metallic support with graphite tape and plasma-coated with a gold–palladium layer under the pulse mode for 20 min. Samples of the composites were prepared by cryogenic microtomy. The composite sheets were cut (perpendicularly to their surfaces and parallel to the xz plane; see Fig. 1) with an RM 2165 microtome from Leica. Samples and knives were cooled to

−150°C. The composite specimens were also plasma-coated with a gold–palladium layer under the pulse mode for 20 min.

Transmission electron microscopy (TEM)

TEM was performed with a JEOL JEM-2100 F field emission gun (80 kV) on thin sections of the composites. The TEM specimens were prepared by either focused ion beam (FIB) cutting or cryogenic microtomy. For the preparation by FIB, a Hitachi FB 2000 instrument (30-kV Ga^+ liquid ion source) was used. FIB is a method recently used for the preparation of microscopic specimens and their three-dimensional (3D) imaging [scanning ion microscopy (SIM)/FIB)]. The FIB sample preparation is a physical process that allows the preparation of surfaces with an ion beam. The beam scans and gradually removes layers of the selected surface by the collision of the ions with the material. By the use of beams with different energies, it is possible to obtain very precise structures. Unlike the microtomy technique, FIB does not induce mechanical stresses on the sample. The method has been mainly used with metallic and semiconducting materials. Its use in polymer sample preparation is delicate because it can induce amorphization of the sample surface,[9,10] scission and/or crosslinking of polymer chains,[11,12] shrinkage of the chains,[13] and modification of the surface chemistry.[14–16] Despite these difficulties, recent publications recommend this method as a useful tool in the preparation of polymer samples.[17–19] The FIB specimens were less than 200 nm thick. For the preparation of the samples by ultramicrotomy, an RM 2165 microtome from Leica was used. The composite sheets were cryogenically cut (perpendicularly to their surfaces) with a diamond knife at an angle of 35°. Both the knife and the samples were cooled to −100°C. Specimens 70 nm thick were put on 400-mesh grids without support. A few of the specimens were decorated with a gold–palladium thin layer under the pulse mode for 2 min to better visualize the morphological differences of the copolymer matrices.

Atomic force microscopy (AFM)

A Nano Scope III multimode atomic force microscope (Dimension 3100, Digital Instruments, Santa Barbara, CA) was used to study the surface morphology of the copolymer composites. The instrument was equipped with a 100 × 100 μm^2 E-scanner and was operated in the tapping mode [tapping-mode atomic force microscopy (TM-AFM)]. The images were recorded under ambient conditions with Veeco MPP 11100 silicon probes with a spring constant of 40 N/m and a resonant frequency of 300 kHz. The tip was oscillated at approximately 98% of the resonant frequency, and the engagement on the surface was performed at 95% of the free oscillation amplitude. Specimens were fixed on a metallic support with AFM adhesive tape. The specimens studied by AFM were prepared by cryogenic microtomy and annealed at 165°C for different periods of time at a heating/cooling rate of 2.5°C/min.

DSC

Thermal analyses of both P/E copolymers and their composites were performed on a TA 2910 instrument. Disklike samples of 5–15 mg were weighed and sealed into TA aluminum DSC pans. The thermal treatment of the DSC samples was carried out under a nitrogen atmosphere. The samples were examined at a scanning rate of 10°C/min by the application of two heating scans and one cooling scan over a temperature range of −150 to 150°C. The melting peaks of the P/E copolymers and those of their composites were taken as the endothermic peaks in the first heating cycle.

RESULTS AND DISCUSSION

SEM morphological analysis of the composite samples prepared by cryogenic microtomy

Figure 2 shows SEM images of composites based on the P/E copolymer with 9 wt % ethylene. The $CaCO_3$ particles are white, and the polymer matrices are gray. Here the specimens were imaged as cut and without any thermal or other pretreatment. No details of the polymer morphology are revealed. Figure 2 does show a uniform dispersion of the $CaCO_3$ particles in the P/E-9 copolymer for all four $CaCO_3$ concentrations used (20, 40, 60, and 80 wt %). Similar results were obtained for the two other P/E copolymers (with 12 and 15 wt % ethylene). As an example, in Figure 3, a uniform dispersion of the $CaCO_3$ particles in the composites with 80 wt % filler is demonstrated. We can see that the polymer matrices uniformly fill the interstices between the filler particles for all the composites. According to these images, the $CaCO_3$ particles are rhombohedra and have lengths between 0.3 and 1.7 μm and an aspect ratio between 1.8 and 3. Similar information is provided by the SEM images of the $CaCO_3$ powder [Fig. 4(a,b)]. Even though the SEM images of the $CaCO_3$ powder show the existence of agglomerates that can reach a 1-mm length [Fig. 4(c)], no such agglomerates were revealed by the SEM images of the 12 composites studied (Figs. 2 and 3). The SEM images of all the composites studied show a random orientation of the $CaCO_3$ particles with respect to the

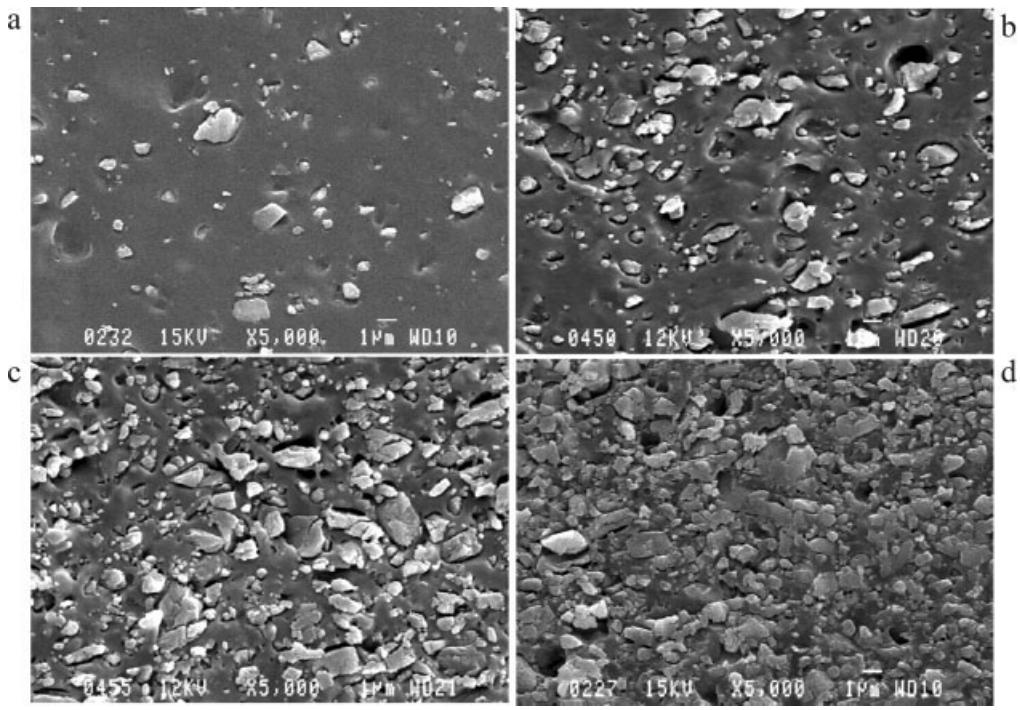

Figure 2 SEM images of the composites based on the P/E-9 copolymer with different $CaCO_3$ contents: (a) 20, (b) 40, (c) 60, and (d) 80 wt % $CaCO_3$.

sample surface, which we recall is perpendicular to the pressed surfaces of the original sheets (Fig. 1). Empty holes are also visible in the SEM images. They are the result of particles falling out during the microtomy preparation. Both the shape of these holes and the traces of the particles on the matrices, observed around the particles, suggest a low adhesion between the P/E copolymers and the $CaCO_3$

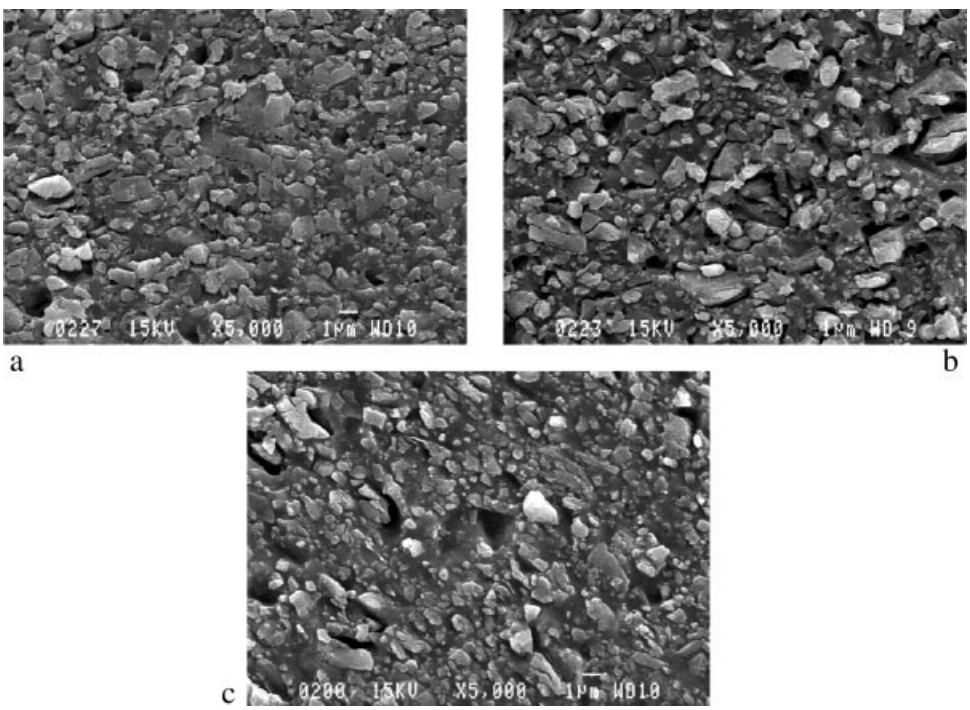

Figure 3 SEM images of the composites with 80 wt % $CaCO_3$ based on the three P/E copolymers: (a) 9, (b) 12, and (c) 15 wt % ethylene.

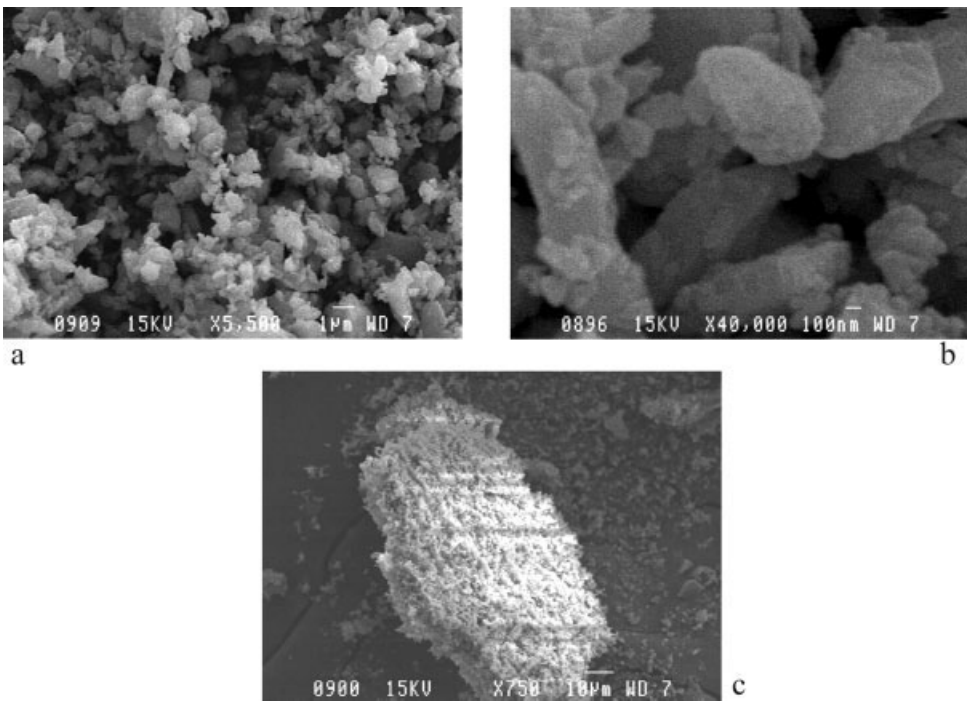

Figure 4 SEM images of $CaCO_3$ powder: (a) 5,500×, (b) 40,000×, and (c) 750 × magnification.

particles. This observation is important, but to understand the nature of the interface in the melt state, further studies must be performed.

SIM/FIB morphological analysis of the composite samples

The samples prepared by FIB were imaged *in situ* by SIM and subsequently also imaged by SEM externally. The SIM/FIB technique allowed us to obtain information about the distribution of the particles in the bulk. The instrument also gives the possibility of changing the sample tilt and recording 3D microscopic images. To minimize modifications of the polymer matrices, the preparation of the samples by FIB was performed in two steps: (1) milling of the samples with higher energy ion beams followed by (2) a clean-up cut realized with a very low energy ion beam. Figure 5 shows the SIM images of the three P/E copolymers filled with 20 wt % $CaCO_3$ during the milling process. Figure 5(a) shows the local melting of the copolymer matrix with 9 wt % ethylene induced by the high-energy ion beams. As a result of the polymer melting, the $CaCO_3$ particles sank deeper in the polymer matrix. More severe modifications of the polymer matrix were induced by the ion beam in the P/E copolymers with higher ethylene contents [Fig. 5(c)]. Figure 5(b) indicates that the flow of the melted P/E-12 copolymer occurred during high-energy milling. The copolymer matrix almost covered the filler particles, leaving only the tops of a few particles visible. In Figure 5(c), several filler particles covered by the melted copolymer with 15 wt % ethylene are visible. The SIM images of the samples taken after the cleaning of the surfaces with the low-energy beam do not show the melting of the polymer anymore. For example, the SIM and SEM images of one final specimen are presented in Figure 6. This indicates that the two-step sample preparation procedure was necessary.

Figure 7 shows the SIM images, taken at tilt angles of 45 and 65°, of the final FIB specimens based on the three P/E copolymers filled with 80 wt % $CaCO_3$. This figure highlights an interesting columnar arrangement of the $CaCO_3$ particles in the polymer matrices. The columnar arrangement is more obvious in the copolymer with 9 wt % ethylene. Additionally, the images in Figure 7 indicate specific interactions of the ion beam with the polymer matrices and with the filler. It is likely that the holes between the columns correspond to the polymer originally separating the particles on vertical planes that was removed during the milling process. The horizontal lines between the particles correspond to the polymer that was not seen by the beam because it was more protected by the particles. It appears that this well-packed $CaCO_3$ arrangement not only is generated by the pressing of the sheets and the shape and small sizes of the $CaCO_3$ particles but could also be related to the crystallinity of the copolymer matrices. In the case of the P/E-15 copolymer (the least crystalline copolymer used in our study),

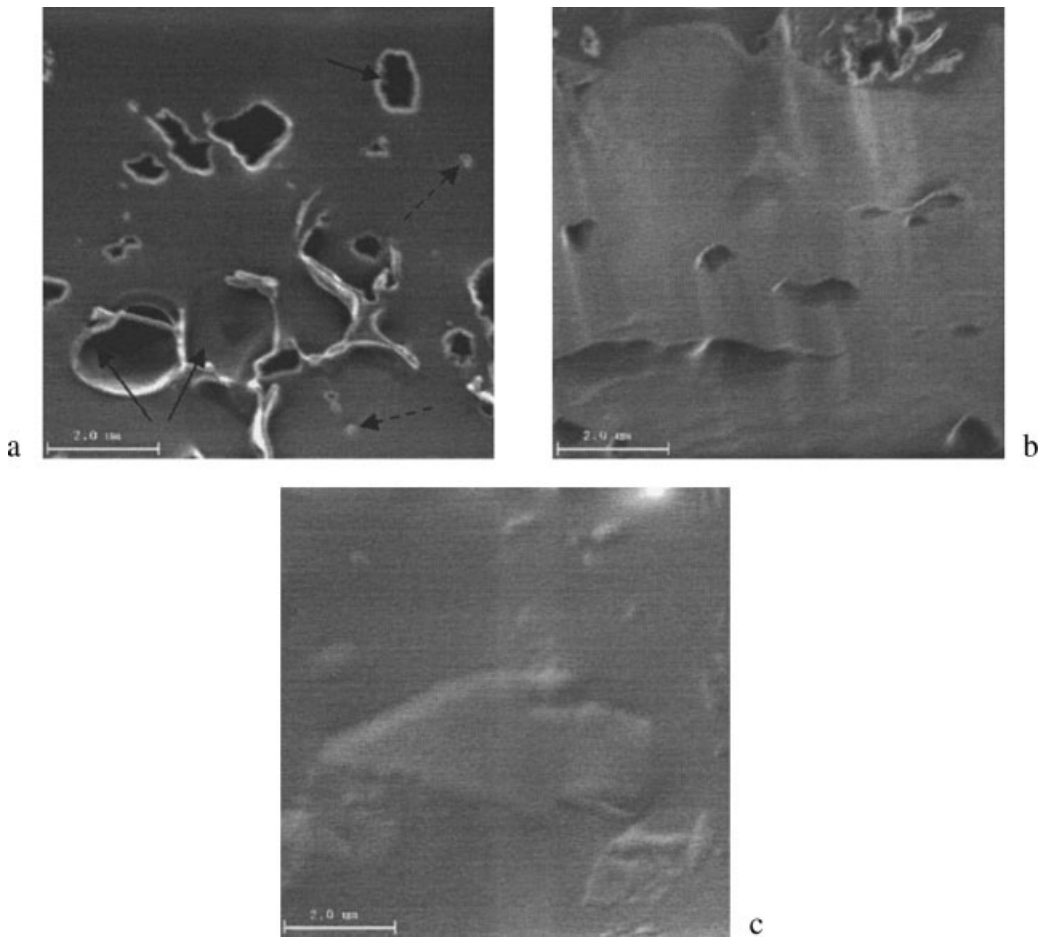

Figure 5 SIM images of the composites with 20% $CaCO_3$ taken during the milling step of the FIB preparation. The P/E matrix had (a) 9, (b) 12, or (c) 15 wt % ethylene. In part a, holes from which particles were removed are indicated with solid arrows, and particles are indicated with dashed arrows.

the particles on the vertical wall of the cut area cannot be clearly seen. The image suggests the existence of a thin layer of the polymer matrix that covers the particles. The image of the sample based on the P/E-15 copolymer was taken at a tilt of 65°. All the images indicate a uniform dispersion of the filler particles in the polymer matrices. The well-packed $CaCO_3$ arrangement in the composites with 80% filler could have an important impact on the rheological behavior of these composites. Therefore, we expect these images to contribute to a better understanding of the rheological behavior of these composites.

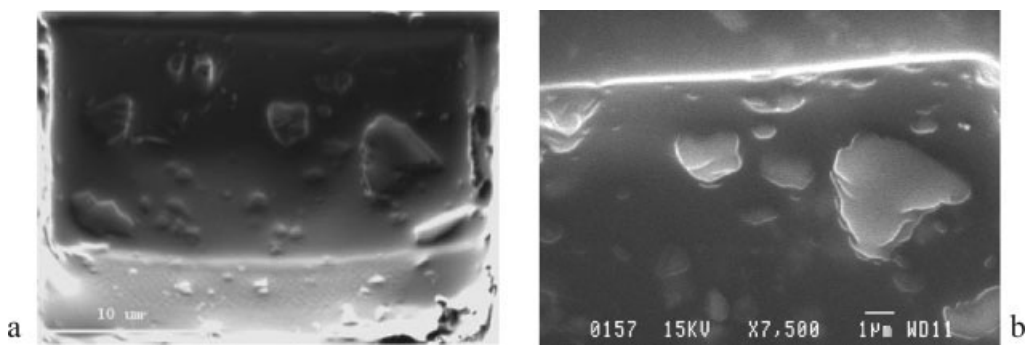

Figure 6 (a) SIM and (b) SEM images of a sample prepared by FIB of the composite based on the P/E-9 copolymer and 20% $CaCO_3$.

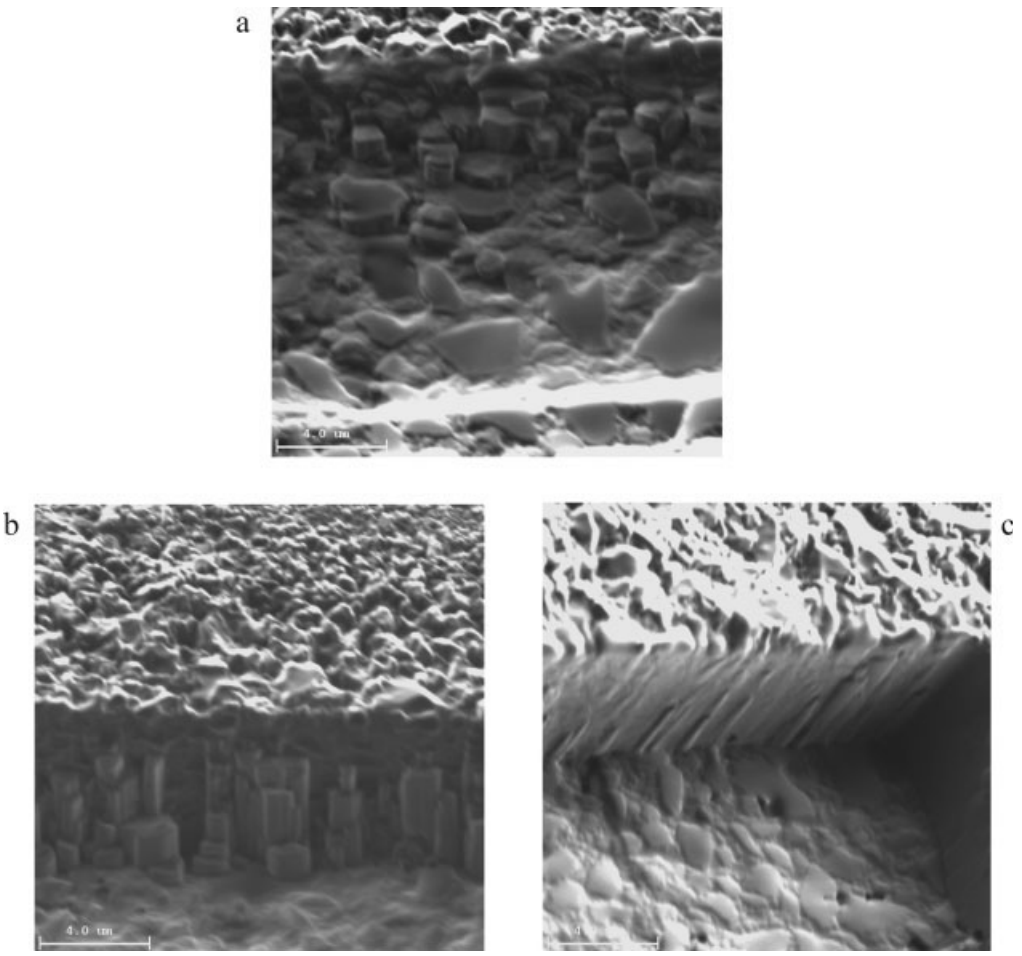

Figure 7 Distribution of the $CaCO_3$ particles in the composites with 80 wt % filler (SIM images). The sample tilt was 45° for (a) the P/E-9 copolymer and (b) the P/E-12 copolymer; the sample tilt was 65° for (c) the P/E-15 copolymer.

TEM morphological analysis

The TEM images of composite specimens prepared by FIB show rhombohedral $CaCO_3$ particles with sizes between 0.35 and 1.7 μm and an aspect ratio between 2.2 and 2.5 uniformly dispersed in the polymer matrices (Fig. 8). The information about the size and aspect ratio agree well with the data obtained by SEM. The darker and lighter areas of the $CaCO_3$ particles' images correspond to different orientations of the $CaCO_3$ crystals with respect to the electron beam [Fig. 8(c,d)]. The TEM images of the specimens prepared by FIB did not reveal information about the morphology of the polymer matrices. The morphology of the polymer matrices and the impact of the filler particles on these morphologies were investigated by electron diffraction. Figure 9 shows an electron diffraction of a sample based on the P/E-12 copolymer. The diffraction results indicate the crystalline structure of $CaCO_3$ [Fig. 9(b)] and an amorphous structure of the polymer matrix [Fig. 9(c)]. Similar results were obtained for the composites based on the other two P/E copolymers. DSC measurements indicate that the three P/E copolymers used in our studies are semicrystalline. Although the crystallinity of these copolymers is not very high and the TEM samples were small ($\sim 14 \times 20$ nm), it is difficult to believe that all three samples studied contained only amorphous polymer chains. In this case, it is necessary to consider the possible modification of the polymer matrices' morphologies either during the FIB preparation or during the diffraction measurements. Therefore, another set of specimens prepared by ultramicrotomy was investigated with TEM. The TEM images of the unstained specimens prepared by ultramicrotomy did not clearly reveal the polymer crystalline structures. Figure 10 shows a TEM image of the 20% $CaCO_3$ composite based on the P/E-9 copolymer, the most crystalline copolymer used in our study. The hatched structure, characteristic of crystalline isopolypropylene and depicted as white lines, is barely visible in this image. This could be the result of the small mass thickness contrast from the polypropylene (30 times less than that of polyethylene[8]) and the relatively high thickness of the sample (70 nm vs 10–20 nm used by other

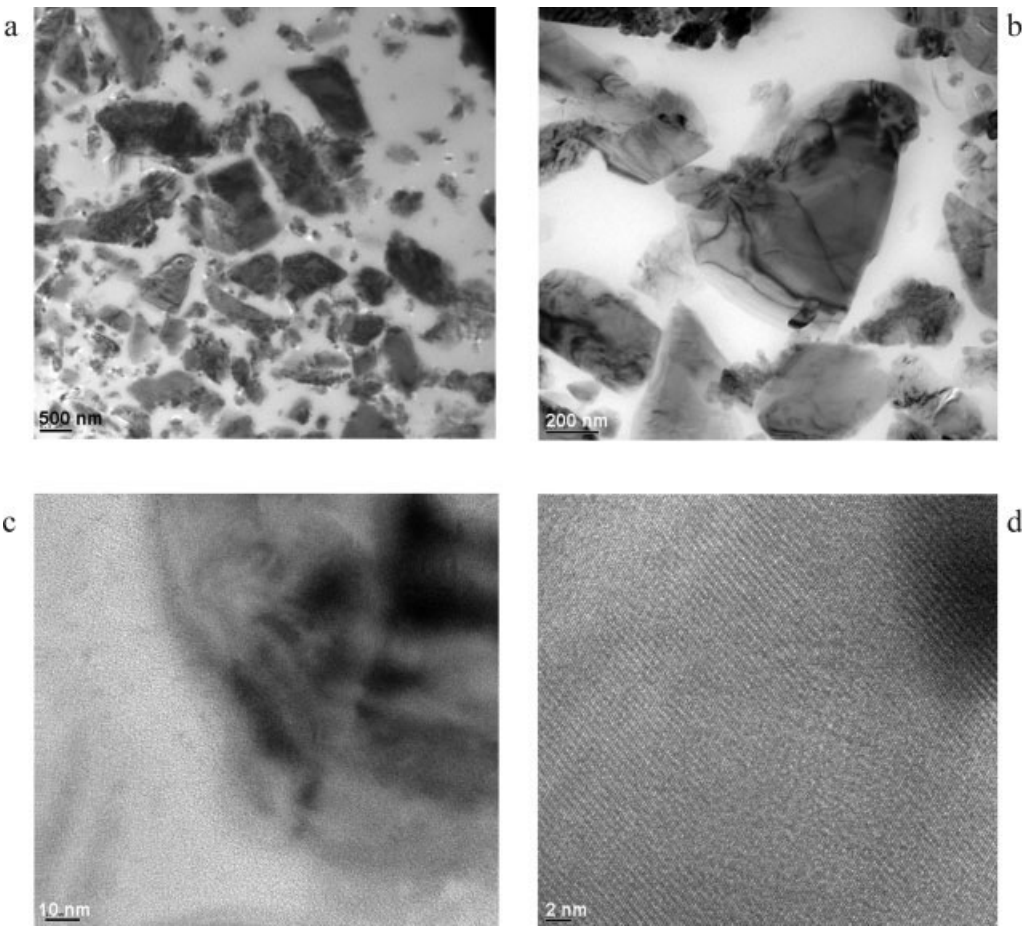

Figure 8 TEM images of a composite based on the P/E-12 copolymer at varying magnification. Images c and d reveal the crystalline structure of $CaCO_3$.

investigators[8]). Presently, the results obtained by both the defocus technique and the use of Au/Pd decorated samples did not bring us more information about the morphologies of the new P/E copolymers. Additionally, we note that the stearate layer, which is expected to be about 2 nm thick, cannot be distinguished in these images.

TM-AFM morphological analysis

The invention and development of scanning probe microscopy and AFM[20–22] provides new capabilities for imaging polymer morphology and mapping multiphase systems based on polymers with nanometer or better spatial resolution. In AFM, a sharp probe (tens of nanometer wide) mounted on a free cantilever end interacts with the sample surface. Among other possibilities, the tip can be in permanent contact with the sample (contact-mode AFM) or can tap the surface with a certain frequency (TM-AFM). TM-AFM has proved to be the most important technique for imaging the morphology of polymeric materials. In TM-AFM, the phase lag of the cantilever oscillation, with respect to the signal sent to the cantilever piezoelectric driver, is monitored simultaneously with the topographic response. The technique provides information about both the amplitude and phase difference. The mapping of the phase during the analysis allows us to go beyond simple topographical imaging and to detect variations in the composition.

Samples prepared by cryogenic microtomy (investigated also with SEM) and annealing were both investigated with TM-AFM. Valuable information regarding the copolymer morphologies was obtained by TM-AFM of the annealed samples. The annealing process enhances the crystallinity. Figure 11 shows the TM-AFM images of a sample based on the P/E-9 copolymer prepared by annealing at 165°C for 30 and 180 min with a heating/cooling rate of 2.5°C/min. For the sample annealed for 30 min, the TM-AFM images [Fig. 11(a–c)] show the existence of many polymer crystals at different growth stages distributed in close parallel rows and an incipient crosshatched structure. The incipient crosshatched structure is revealed more clearly in Figure 11(b),

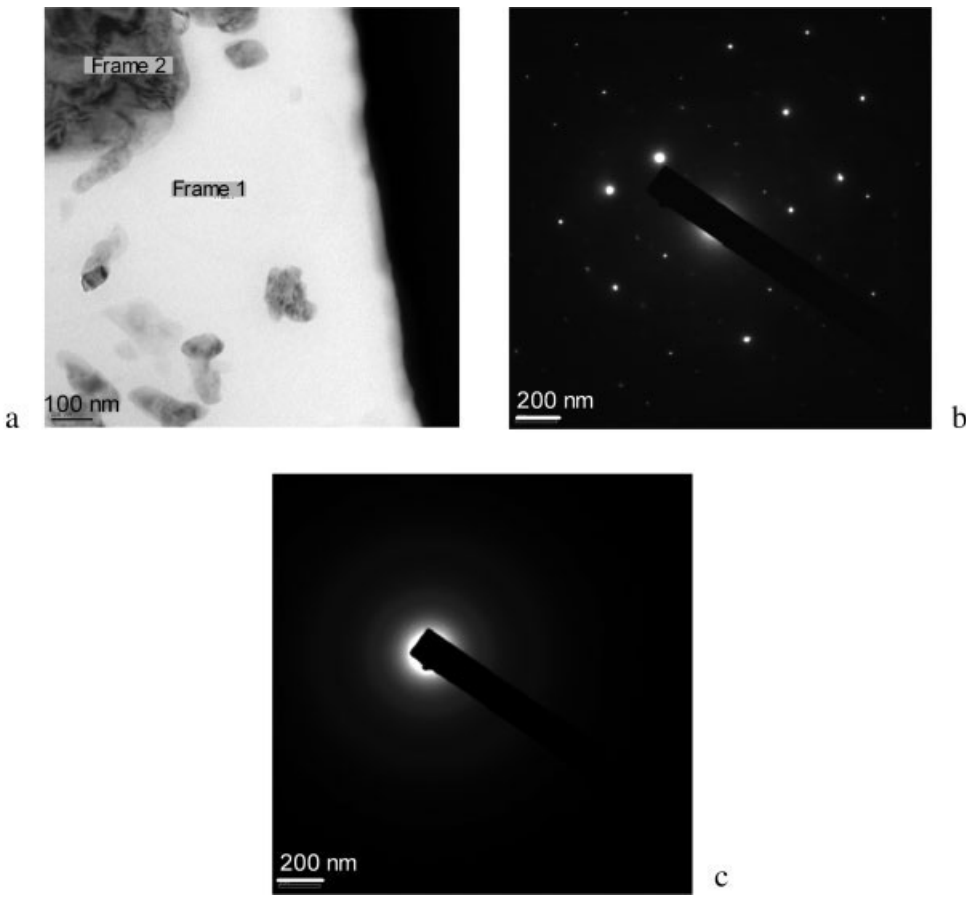

Figure 9 Electron diffraction of a composite based on the P/E-12 copolymer: (a) the investigated area of the sample (frame 1 corresponds to image b, and frame 2 corresponds to image c), (b) the electron diffraction of the copolymer matrix, and (c) the electron diffraction of $CaCO_3$.

whereas Figure 11(c) shows better the polymer crystals. The TM-AFM images of the samples annealed for 180 min reveal a morphology characteristic of semicrystalline copolymers in which both crystalline and amorphous phases coexist. Figure 11(d) shows a crystalline phase characterized by a dense crosshatched structure. The crystalline lamellae are 100–400 Å thick and 300 Å apart. The interlamellar amorphous zones between the closely packed lamellae are 0.9–1.3 μm. The crosshatched morphology with lamellar branching at defined angles is evidence for the presence of monoclinic α-isotactic polypropylene. The observation of thick dominant lamellae, branching with an angle of 80°, and thin branches agrees well with the results of previous morphological studies on isopolypropylene.[23,24] In the upper, right-hand corner of Figure 11(d), an amorphous area can be seen in which the existence of either deeper crystalline entities or filler particles beneath the amorphous phase is suggested.

The TM-AFM images of the composite based on the P/E-12 copolymer exhibit a markedly different morphology (Fig. 12). The few crystals visible in the image of the sample annealed for 30 min are not arranged in close parallel rows [Fig. 12(b)]. The orientation of the crystals in parallel rows could still exist, but if the distance between the rows is bigger, it would not be observed here because of the scan size. It is also likely that the crystallization at 165°C of this copolymer is slower than that of the P/E-9 copolymer. The presence of more ethylene units, which disrupt the crystal lattice formation, could require more complex movements of the chains and thus longer time for the formation of crystals. The sample annealed for 180 min shows crystalline lamellae that are short, blocklike, or curved because of the frequent imperfections induced by the ethylene units. As a result of these frequent imperfections, the isotactic sequences are shorter. The interlamellar amorphous zones between the packed lamellae are 9.5–35 μm. In this case, the crosshatched lamellar branching, typical for an α-isotactic polypropylene structure, was not observed. The absence of crosshatching indicates that the polymer chains possess a significant number of defects. These defects are derived from ethylene, which could be excluded from the chain-folded lamellae. The participation of ethylene units in the propylene crystalline

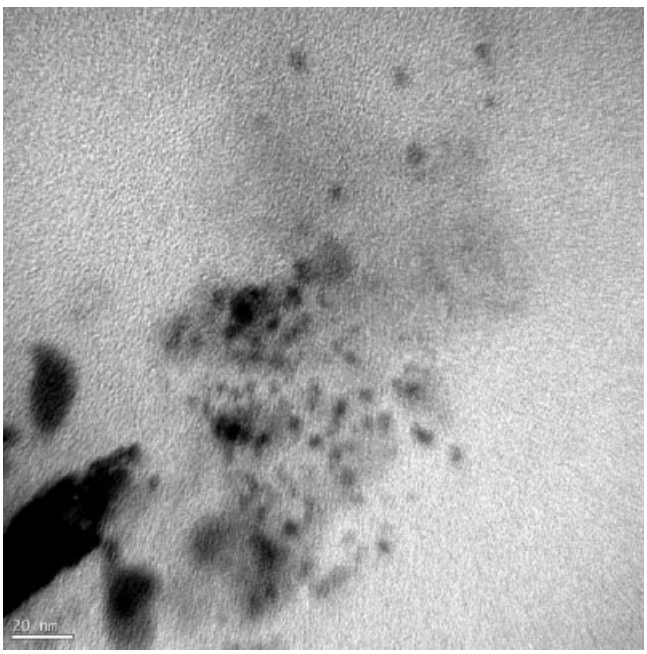

Figure 10 TEM image of a composite sample based on the P/E-9 copolymer and 20 wt % filler. The sample was prepared by cryogenic microtomy.

lattice is a subject of interest. On the basis of molecular mechanics calculations for model compounds[25] or on the invariance of the crystallinity and the crystal thickness with increasing ethylene content,[26] certain authors have concluded that the ethylene units are partially included in the crystal. In other reports, the decrease of the melting temperature with increasing comonomer concentration[27] has led to the conclusion that the ethylene units are rejected from the crystal. The possible high concentration of the ethylene defects at the crystalline/noncrystalline interface and the modification of the isotactic polypropylene chain conformation in the vicinity of the ethylene defects have also been investigated. An interesting study of the morphological partition of ethylene defects in random P/E copolymers[28] led to the conclusion that the ethylene defects are not highly concentrated at the crystalline/noncrystalline interface and that the isotactic polypropylene chain conformation in the crystalline regions in the vicinity of the ethylene defect is not modified.

The TM-AFM images of the annealed composites based on the P/E-15 copolymer revealed interesting information about the morphology of this copolymer. For the sample annealed for 30 min, Figure 13(a) shows a few small crystals with irregular shapes. The crystals do not have the same shape as the isopropylene crystals shown by the TM-AFM images of the P/E-9 and P/E-12 copolymers [Figs. 11(c) and 12(b)]. This seems to be reasonable if we take into account the differences in the melting points revealed by the DSC study. The P/E copolymers with 9 or 12% ethylene have melting points characteristic of isopolypropylene with short tactic units at 132 and 134°C, whereas the copolymer with 15% ethylene presents a melting point at 125°C. The TM-AFM images of the samples annealed for 180 min at 165°C [Fig. 13(c,d)] suggest a mainly amorphous polymer matrix with groups of small crystals located preferentially on top of the $CaCO_3$ particles. The size and shape designed by the groups of crystals correspond to the $CaCO_3$ particle dimensions and shape. The four regions with dark outlines [one of them being highlighted in white in Fig. 13(d)] are likely top parts of bigger crystals protruding from the polymer. Their well-defined edges are due to the difference in height between the areas of the polymer existing on either side of the edges in question, as shown by the section analysis. The 3D images of this sample suggest a similar interpretation for the upper region highlighted in white.

Figure 14 compares the individual crystals of the three copolymers. The P/E-9 copolymer shows crystals with different sizes and shapes [Fig. 14(a)]. The crystals have broad size and shape distributions as a result of the randomly distributed ethylene units in the copolymer chains. Most of the crystals are pretzel-like with a closed or open texture. The thickness of the pretzel-like crystals is relatively uniform. The P/E-15 copolymer [Fig. 14(b)] shows a few crystals, some of them being grouped. This grouplike arrangement must be the result of the presence of a $CaCO_3$ particle, underneath the polymer, which acts as a nucleating agent for the copolymer crystallization. The crystals have either a closed or open texture and do not have a pretzel-like shape. The transversal wall, which can be seen in the crystals of the P/E-9 copolymer, is not complete in the case of the P/E-15 copolymer. Only the beginning and end of the transversal wall can be seen. Also, in this case, the thickness of the crystals is not uniform. Figure 14(c) shows a 3D image of the individual crystals of the P/E-12 copolymer. Most of the crystals have an open texture, and the thickness of the crystals is not uniform. Some of the crystals have a middle wall, similar to the crystals of the P/E-9 copolymer; others have only the beginning and end of the middle wall, similar to the crystals of the P/E-15 copolymer; and others have in the middle several parallel transversal walls. This new shape of the crystals with a few parallel transversal walls implies that the thickness of the crystals is the result of the existence of different parallel crystallite rows that are so close together that they cannot be seen individually. The differences between the number of the crystals, their shapes, and their sizes, revealed by the 2-μm scans of the three P/E copolymers, are generated by the

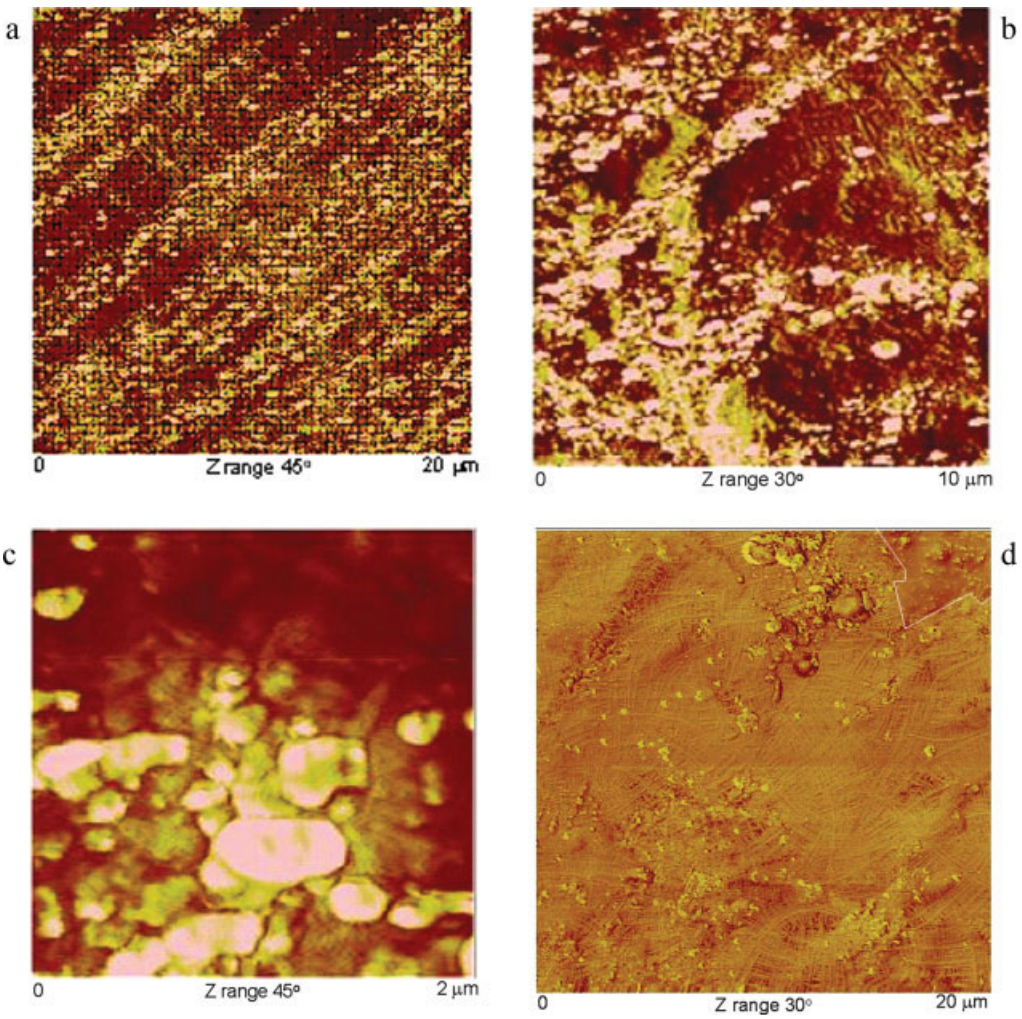

Figure 11 TM-AFM phase images of composites with 20% filler and the P/E-9 copolymer. The samples were prepared by annealing at 165°C: (a–c) 30 and (d) 180 min of annealing. The rate of heating/cooling was 2.5°C/min. [Color figure can be viewed in the online issue, which is available at www.interscience.wiley.com.]

increase in the ethylene content. The higher ethylene content decreases the number of crystals and increases the amount of noncrystallizable material within the crystal boundaries, leading to the formation of nonuniform, open-textured crystals with many defects.

The TM-AFM images of the composite specimens prepared by annealing also revealed the presence of $CaCO_3$ particles in the polymer matrices. In most cases, the particles were covered by the polymer matrix during the annealing preparation. Figure 15(a) shows a $CaCO_3$ particle covered by polymer crystals during the annealing of the P/E-12 copolymer filled with 20 wt % filler. The sample was annealed for 30 min at 165°C. The presence of crystals on the particle surface was also shown by the TM-AFM images of the P/E-9 composite that was annealed for 180 min [Fig. 15(b)]. Figure 15(b) shows both the crystalline morphology of the copolymer and a $CaCO_3$ particle. It appears that the crosshatched structure close to the particle is slightly different from that further away. It is difficult to attribute this different morphology to the presence of the particle because a similar morphology can be seen in areas without particles (see the close right and left upper areas). It is known that molten polymer molecules close to solid surfaces adopt a more aligned conformation than that in the bulk, but in our case, neither the TM-AFM images nor the TEM images revealed differences in the polymer morphology that could be attributed to this phenomenon.

Our study by TM-AFM did not highlight the stearate monolayer around the $CaCO_3$ particles despite its thickness of $\sim$ 2.6 nm. This is quite normal if we think that most of the particles are covered with polymer during the sample preparation. It seems that the possibility of seeing this layer is higher in the samples prepared by ultramicrotomy. However, the roughness of these samples made it difficult to

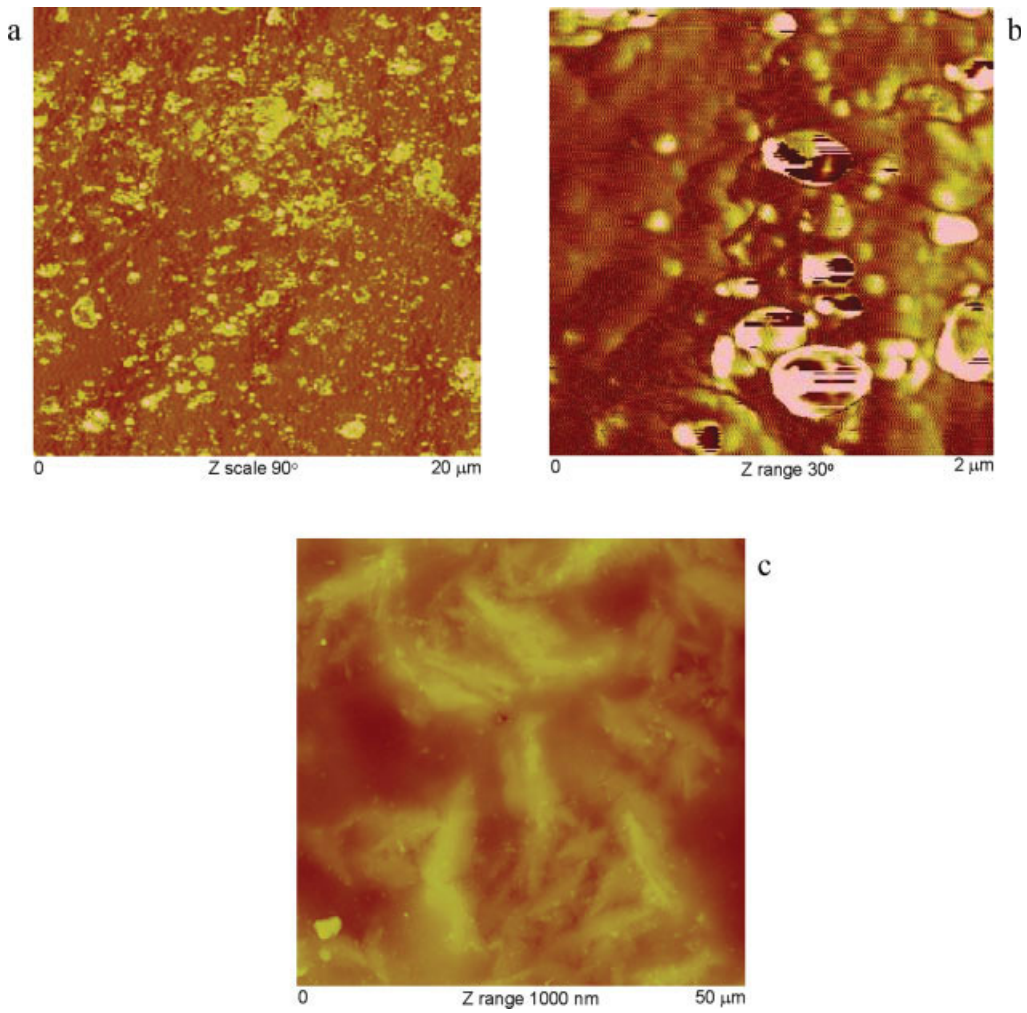

Figure 12 TM-AFM images of composites of P/E-12 and 20% filler after annealing at 165°C: (a,b) TM-AFM phase images of a sample annealed for 30 min and (c) a TM-AFM height image of a sample annealed for 180 min. The rate of heating/cooling was 2.5°C/min. [Color figure can be viewed in the online issue, which is available at www.interscience.wiley.com.]

locate the particles with TM-AFM. In the TEM images, the particle edges are sharply depicted, but this is most likely the result of the abrupt refractive index change. Difficulties in the visualization of the surface contact between the $CaCO_3$ particle covered with stearate and the copolymer matrix is also due to the very similar chemical structures of the two organic phases in contact and, as a result, very similar surface energies.

Thermal analysis of the P/E copolymers and their composites

Thermal analysis of the three P/E copolymers and their composites was carried out by DSC. The DSC curves of the three P/E copolymers display broad melting endotherms. In the first heating scan of the P/E-9 copolymer, three melting peaks at 56, 108, and 134°C were recorded. For the copolymers with 12 or 15% ethylene, only two melting peaks at 52 and 132°C and at 50 and 125°C, respectively, were observed (Fig. 16). The crystallinity of the three P/E copolymers was found to be approximately 28.7, 18.2, or 9.3%, respectively. They were calculated by the division of their enthalpy of fusion by 165 J/g, which is the enthalpy of fusion for a perfect crystal of polypropylene.[29] As a result of the increase in the ethylene content from 9 to 15%, the glass-transition temperature decreased from −24 to −34°C.

The DSC analysis of the 12 composites indicates that $CaCO_3$ is a weak nucleating agent for all three copolymers (Figs. 17 and 18). Figure 17 shows the heat of fusion per gram of polymer for all 12 composites. We can see evidence of slightly higher crystallinity for all three copolymers as $CaCO_3$ is added. This effect is more pronounced at lower ethylene

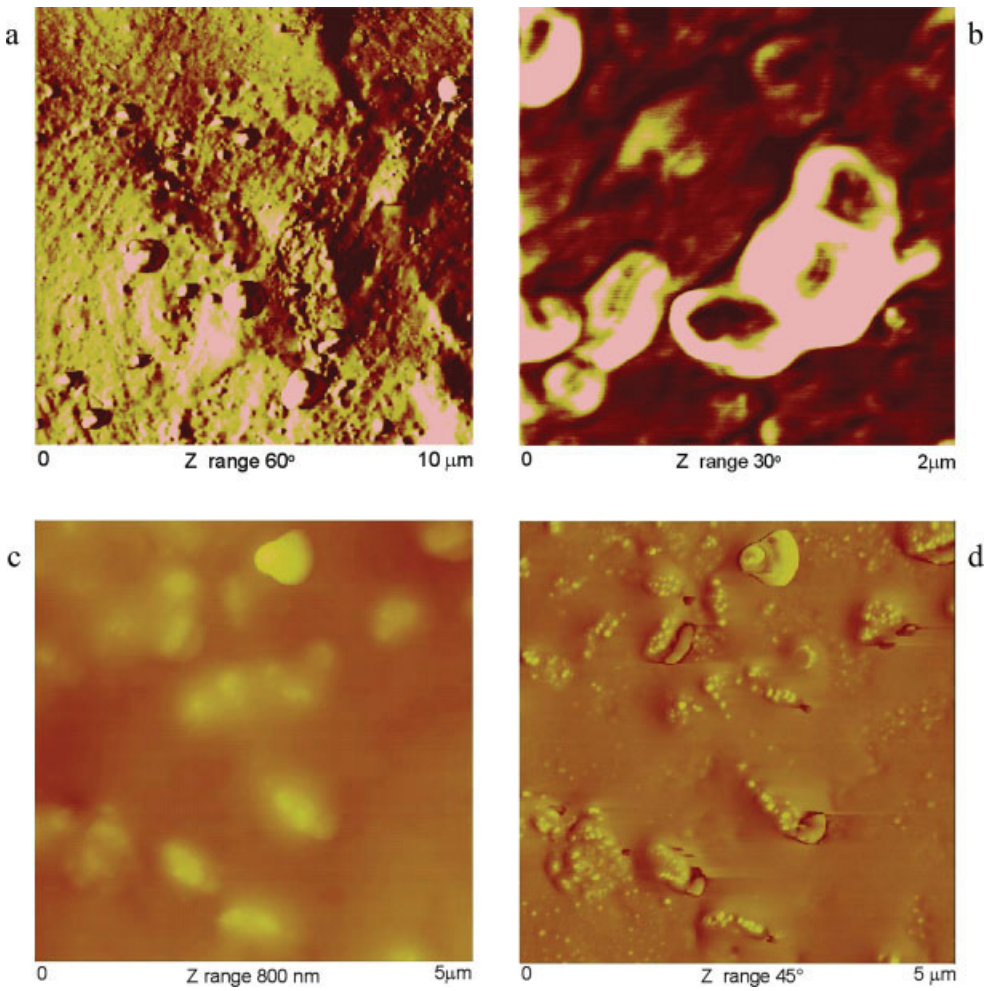

Figure 13 TM-AFM images of composites with 20% filler and the P/E-15 copolymer. The samples were prepared by annealing at 165°C: (a,b) TM-AFM phase images of a sample annealed for 30 min and (c,d) images of a sample annealed for 180 min. The rate of heating/cooling was 2.5°C/min. [Color figure can be viewed in the online issue, which is available at www.interscience.wiley.com.]

contents as expected. The analysis of the cooling scans showed that the P/E copolymers undergo supercooling, which is the difference between the melting temperature and the temperature at which crystallization occurs. The pure P/E copolymers have melting peaks at 134 (P/E-9), 130 (P/E-12), and 125°C (P/E-15) and crystallize at about 57, 41, and 13°C, respectively. For the composites, the crystallization temperatures are dramatically higher because of the nucleating effect of the $CaCO_3$ particles, as shown in Figure 18. Interestingly, the reduction in supercooling is strongest in the case of the composites based on P/E-15, which is mainly amorphous (9.3% crystallinity), and weakest in the case of P/E-9, which has the highest crystallinity. Moreover, the nucleating effect of the particles essentially saturates by 20% $CaCO_3$, and further increases in the filler content result in few changes in the crystallization temperature.

The results of the DSC study (Figs. 17 and 18) indicate that although the rate of nucleation is affected by the particles, the final crystallinity in the copolymer matrix is determined mainly by the ethylene content. This small influence could be explained by the very weak interactions at the interface of the copolymer matrix and $CaCO_3$ particles (i.e., London forces). The stearate coating increases the wettability of the $CaCO_3$ particles, leading to their good dispersion in the polymer matrices, and decreases the adhesion of the matrix to the particles' surface.

CONCLUSIONS

A study of composites based on the new Dow P/E copolymers has shown that the $CaCO_3$ particles are uniformly dispersed in the copolymer matrices for all three P/E copolymers and for all four concentra-

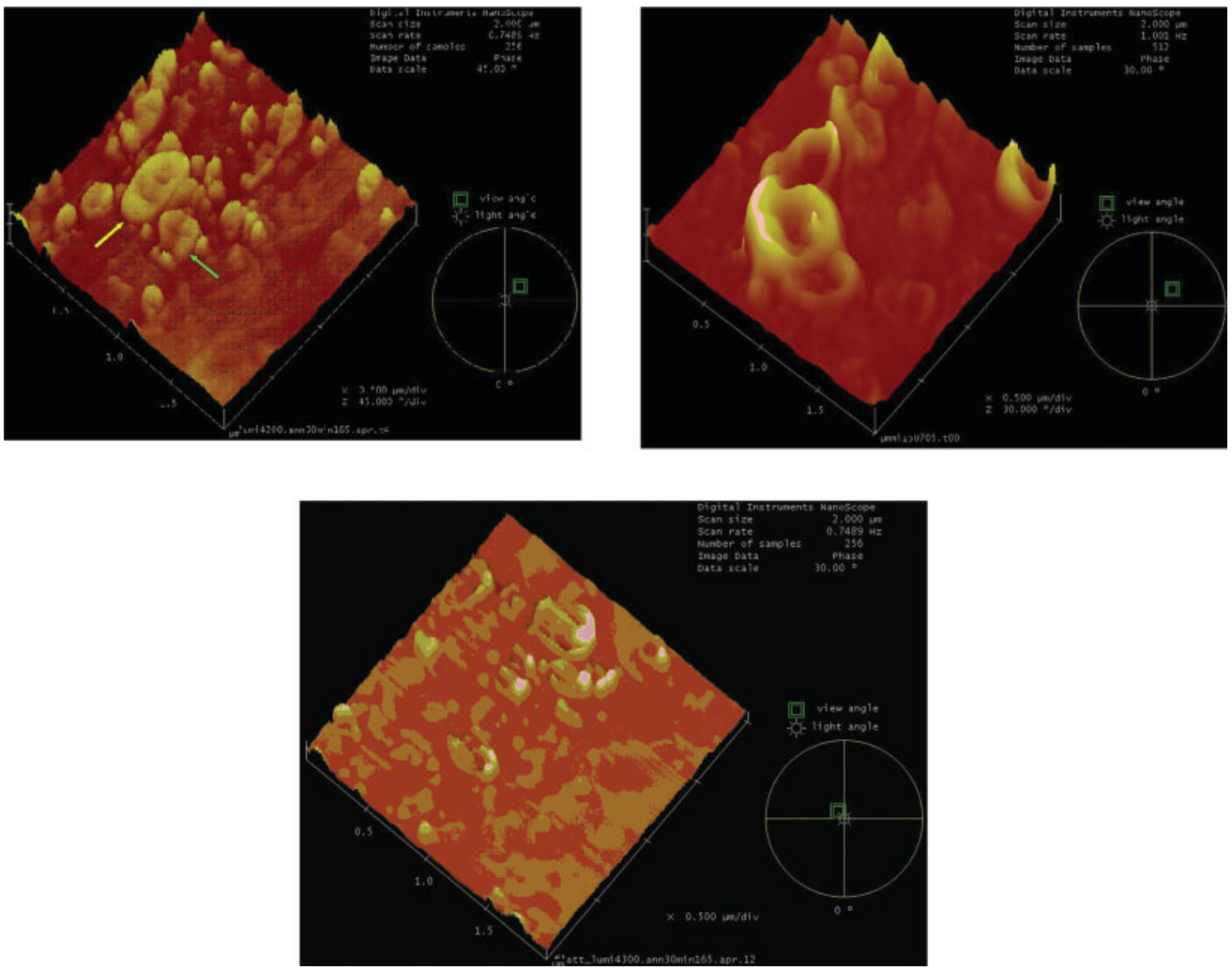

Figure 14 3D TM-AFM images of individual crystals of the three P/E copolymers studied. [Color figure can be viewed in the online issue, which is available at www.interscience.wiley.com.]

tions of the filler. The particles are randomly oriented with respect to the surface of the polymer matrices. The empty holes from which particles have fallen from the copolymer matrices in the cut samples suggest a low adhesion between the polymer matrices and the filler, corresponding to a large con-

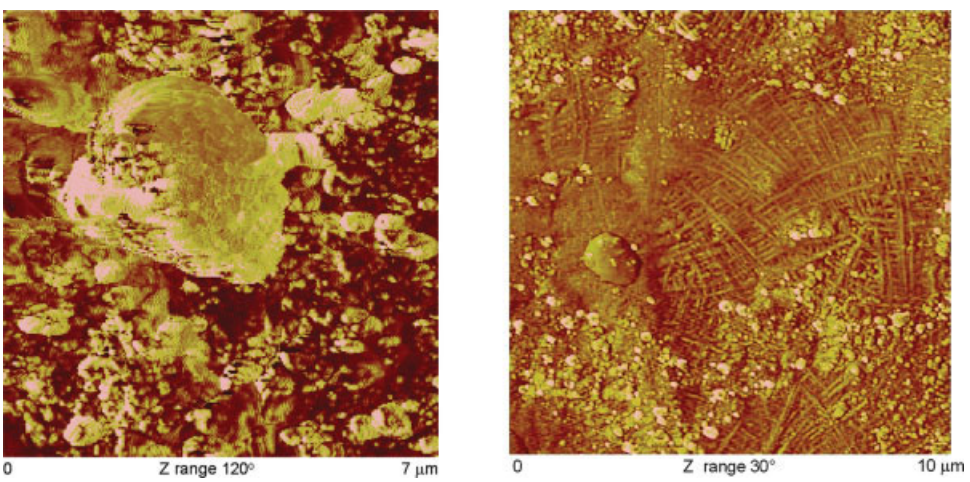

Figure 15 TM-AFM images of $CaCO_3$ particles in composites annealed at 165°C: (a) P/E-12 matrix and (b) P/E-9 matrix. [Color figure can be viewed in the online issue, which is available at www.interscience.wiley.com.]

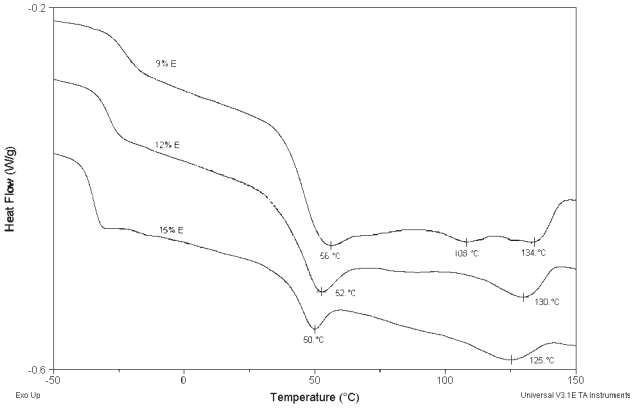

Figure 16 DSC traces of the pure P/E copolymers (first run, 10°C/min heating rate).

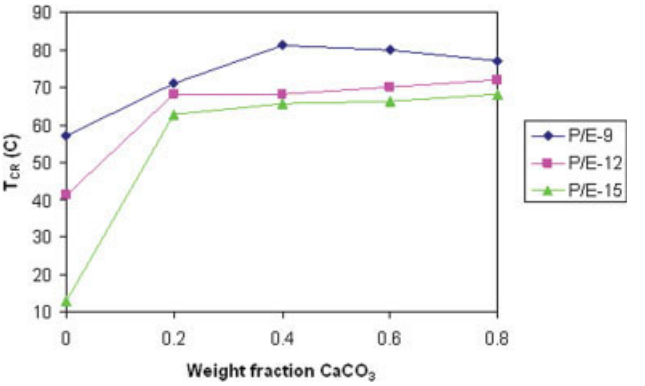

Figure 18 Influence of $CaCO_3$ on the crystallization temperature (T_{CR}) of the P/E copolymers (DSC, 10°C/min cooling rate). [Color figure can be viewed in the online issue, which is available at www.interscience.wiley.com.]

tact angle between them. This low adhesion is due to the nonreactive stearate coating of the $CaCO_3$ particles. The SIM images indicate a well-packed structure of the $CaCO_3$ particles in the composites with 80 wt % filler.

All three copolymer matrices are semicrystalline, but they have different morphologies. When crystallized from the melt, they show morphologies characteristic of classical semicrystalline polymers. The TM-AFM images of the annealed composite with 9 wt % ethylene depicted the presence of spherulites in different stages of development, lamellae, and a crosshatched structure characteristic of the α-isopolypropylene. An increase in the ethylene content led to a decrease in the crystallinity as expected. As a result, the crosshatching was not present in the copolymers with 12 or 15% ethylene. Also, in these two copolymers, the crystalline entities were smaller, and the nucleation density was low. The stearate-treated $CaCO_3$ particles have a small influence on the thermal behavior of the P/E copolymers. The stearate-treated $CaCO_3$ particles act as nucleating agents for the copolymer crystallization, reducing supercooling but not increasing the final crystallinity significantly. This nucleation effect is stronger at higher ethylene contents.

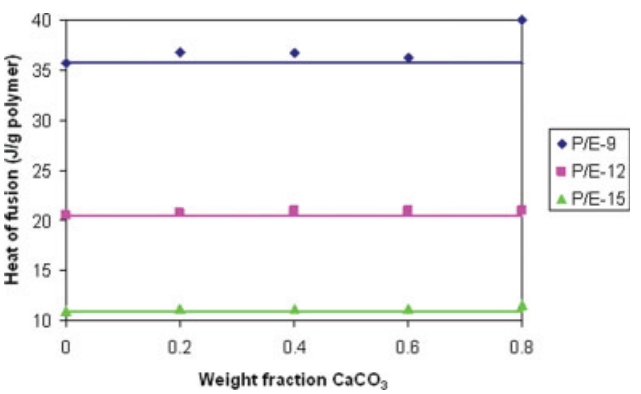

Figure 17 Heat of fusion per gram of polymer as a function of the $CaCO_3$ concentration (DSC study, 10°C/min heating rate, second heating). The horizontal lines show the enthalpy of fusion of the pure copolymers. [Color figure can be viewed in the online issue, which is available at www.interscience.wiley.com.]

References

1. Deming, T. J. J Polym Sci Part A: Polym Chem 2000, 38, 3011.
2. Deming, T. J. Nature 1997, 390, 386.
3. Ovitt, T. M.; Coates, G. W. J Am Chem Soc 1999, 121, 4072.
4. Tian, J.; Coates, G. W. Angew Chem Int Ed Engl 2000, 39, 3626.
5. Brintzinger, H. H.; Fischer, D.; Mulhaupt, R.; Rieger, B.; Waymouth, R. M. Angew Chem Int Ed Engl 1995, 34, 1143.
6. Collette, J. W.; Ovenall, D. W.; Buck, H. W.; Ferguson, R. Macromolecules 1989, 22, 3858.
7. Bravakis, A. M.; Pigeon, L. E.; Collins, S. Macromolecules 1998, 31, 1000.
8. Swogger, K. W.; Poon, B.; Ansems, P.; Chum, S.; Hiltner, A.; Baer, E. Soc Plast Eng Annu Tech Conf Tech Pap 2003, 49, 1768.
9. Roche, E. J.; Thomas, E. L. Polymer 1981, 22, 333.
10. Said, M. A.; Balik, C. M.; Carlson, J. D. J Polym Sci Part B: Polym Phys 1988, 26, 1457.
11. Musumeci, P.; Calcagno, L.; Percolla, R.; Foti, G. J Appl Phys 1995, 77, 3766.
12. Schnabel, W.; Klaumünzer, S.; Sotobayashi, H.; Asmussen, F.; Tabata, Y. Macromolecules 1984, 17, 2108.
13. Calcagno, L.; Percolla, R.; Masciarelli, D.; Foti, G. J Appl Phys 1993, 74, 7572.
14. Merhari, L.; Belorgeot, C.; Moliton, J. P. J Vac Sci Technol B 1991, 9, 2511.
15. Terrasi, A.; Foti, G.; Hwu, Y.; Margarirondo, G. J Appl Phys 1991, 70, 1885.
16. Beamson, G.; Clark, N. W.; Hayes, N. W.; Law, D. S.-L.; Siracusa, V.; Recca, A. Polymer 1996, 37, 379.
17. Calcagno, L.; Compagnini, G.; Foti, G. Nucl Instrum Methods B 1992, 65, 413.

18. White, H.; Pu, Y.; Rafailovich, M.; Sokolov, J.; King, A. H.; Gianuzzi, L. A.; Urbanik-Shannon, C.; Kempshall, B. W.; Eisenberg, A.; Schwarz, S. A.; Strzhemechny, Y. M. Polymer 2001, 42, 1613.
19. Vergilio, N.; Favis, B. D.; Pépin, M.-F.; Desjardins, P.; L'Espérance, G. Macromolecules 2005, 38, 2368.
20. Kajiyama, T.; Tanka, K.; Ge, S. R.; Takahara, A. T. Prog Surf Sci 1996, 52, 1.
21. Chen, H. Y.; Cheung, Y. W.; Hilner, A.; Baer, E. Polymer 2001, 42, 7819.
22. Lazzaroni, R.; Leclère, P.; Couturiaux, A.; Parente, V.; François, B.; Brédas, J. L. Synth Met 1999, 102, 1279.
23. Janimak, J. J.; Cheng, S. Z. D.; Giusti, P. A.; Hsieh, E. T. Macromolecules 1991, 24, 2253.
24. Schönherr, H.; Wiyatno, W.; Frank, C. W.; Fuller, G. G.; Gast, A. P.; Pople, J. A.; Waymouth, R. M. Macromolecules 2002, 35, 2564.
25. Starkweather, H. W., Jr.; Van-Catledge, F. A.; MacDonald, R. N. Macromolecules 1982, 15, 1600.
26. Laihonen, S.; Gedde, U. W.; Werner, P.-E.; Westdahl, M.; Jääskeläinen, P.; Martinez-Slazar, J. Polymer 1997, 38, 371.
27. Feng, Y.; Hay, J. N. Polymer 1998, 39, 6589.
28. Alamo, R. G.; VanderHart, D. L.; Nyden, M. R.; Mandelkern, L. Macromolecules 2000, 33, 6094.
29. Wunderlich, B. Macromolecular Physics: Crystal Melting; Academic Press: New York, 1980; Vol. 3, p 63.